J|A|C|S
ARTICLES
Published on Web 08/04/2006

Quadruplex-Based Molecular Beacons as Tunable DNA Probes

A. Bourdoncle,[†,‡] A. Estévez Torres,[†] C. Gosse,[*,§] L. Lacroix,[‡] P. Vekhoff,[‡] T. Le Saux,[†] L. Jullien,[*,†] and J.-L. Mergny[*,‡]

Contribution from the Département de Chimie, CNRS UMR 8640, École Normale Supérieure, 24 rue Lhomond, 75231 Paris Cedex 05, France, Laboratoire de Biophysique, Muséum National d'Histoire Naturelle, USM503, INSERM U 565, CNRS UMR 5153, 43 rue Cuvier, 75231 Paris Cedex 05, France, and Laboratoire de Photonique et de Nanostructures, LPN-CNRS, Route de Nozay, 91460 Marcoussis, France

Received February 2, 2006; E-mail: Ludovic.Jullien@ens.fr

Abstract: Molecular beacons (MBs) are fluorescent nucleic acid probes with a hairpin-shaped structure in which the 5′ and 3′ ends are self-complementary. Due to a change in their emissive properties upon recognition with complementary sequences, MBs allow the diagnosis of single-stranded DNA or RNA with high mismatch discrimination, in vitro and in vivo. Whereas the stems of MB hairpins usually rely on the formation of a Watson−Crick duplex, we demonstrate in this report that the preceding structure can be replaced by a G-quadruplex motif (G4). Intramolecular quadruplexes may still be formed with a central loop composed of 12 to 21 bases, therefore extending the sequence repertoire of quadruplex formation. G4-MB can efficiently be used for oligonucleotide discrimination: in the presence of a complementary sequence, the central loop hybridizes and forms a duplex that causes opening of the quadruplex stem. The corresponding G4-MB unfolding can be detected by a change in its fluorescence emission. We discuss the thermodynamic and kinetic opportunities that are provided by using G4-MB instead of traditional MB. In particular, the intrinsic feature of the quadruplex motif facilitates the design of functional molecular beacons by independently varying the concentration of monovalent or divalent cations in the medium.

1. Introduction

Molecular beacons (MBs) are oligonucleotide probes that become fluorescent upon binding to a complementary sequence of single-stranded nucleic acid. Since their discovery in 1996,[1] they have been extensively used in homogeneous hybridization assays in vitro and in vivo.[2,3] An MB contains a stem and a loop. In the MB closed state, the stem brings to proximity a fluorescent dye and a quencher located at both ends of the oligonucleotide: the fluorescence emission from the dye is consequently quenched.[4,5] The loop region, and sometimes also a part of the stem in the so-called shared-stem constructs,[6] is the target recognition portion of the MB. Upon binding to a matching target region, the stem opens and the distance between the fluorescent dye and the quencher increases, enabling fluorescence emission to be detected (Figure 1).

MB design involves considerations related to both fluorescence detection and molecular recognition. An efficient detection requires choosing an appropriate fluorescent dye/quencher combination to maximize the alteration of the fluorescence emission upon target binding.[1,7,8] An optimized recognition relies on maximizing the association extent with the complementary target regarding mismatched sequences. Engineering constraints here are numerous to ensure, at the same time, a significant hybridization at a given target concentration and the emphasis on the free-energy penalty associated with mismatched base pairs. In their pioneering work on stringency clamps, Roberts and Crothers suggested that the stability of the alternative secondary structure of the probe (here the MB hairpin) should be between the ones of the perfect and of the defect complexes: matched duplexes would then form, whereas mismatched ones would not due to the competing intramolecular folding of the probe.[9] MBs allow achievement of the preceding thermodynamic condition quite easily because different free parameters such as the stem length and sequence, as well as the loop length, can be tuned independently.[10] As it will be shown in the present report, one can finely play with a larger number of optimizing parameters when using structured DNA probes that involve G-quadruplexes.

[†] École Normale Supérieure.
[‡] Muséum National d'Histoire Naturelle.
[§] LPN-CNRS.

(1) Tyagi, S.; Kramer, F. R. *Nat. Biotechnol.* **1996**, *14*, 303−308.
(2) Broude, N. E. *Trends Biotechnol.* **2002**, *20*, 249−256.
(3) Tan, W.; Wang, K.; Drake, T. J. *Curr. Opin. Chem. Biol.* **2004**, *8*, 547−553.
(4) Tyagi, S.; Bratu, D. P.; Kramer, F. R. *Nat. Biotechnol.* **1998**, *16*, 49−53.
(5) Bernacchi, S.; Mely, Y. *Nucleic Acids Res.* **2001**, *29*, e62.
(6) Tsourkas, A.; Behlke, M. A.; Bao, G. *Nucleic Acids Res.* **2002**, *30*, 4208−4215.
(7) Dubertret, B.; Calame, M.; Libchaber, A. *Nat. Biotechnol.* **2001**, *19*, 365−370.
(8) Marras, S. A. E.; Kramer, F. R.; Tyagi, S. *Nucleic Acids Res*. **2002**, *30*, e122.
(9) Roberts, R. W.; Crothers, D. M. *Proc. Natl. Acad. Sci. U.S.A.* **1991**, *88*, 9397−9401.
(10) Bonnet, G.; Tyagi, S.; Libchaber, A.; Kramer, F. R. *Proc. Nat. Acad. Sci. U.S.A.* **1999**, *96*, 6171−6176.

10.1021/ja0608040 CCC: $33.50

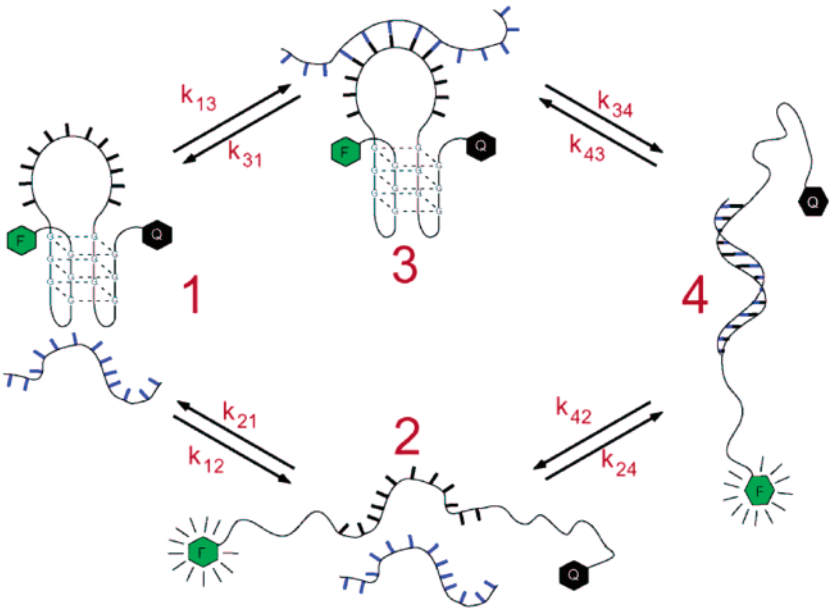

Figure 1. Competing pathways for molecular recognition between an oligonucleotide target and a G4-based molecular beacon (G4-MB). In the upper pathway, partial recognition is followed by invasion that leads to beacon opening. In contrast, binding of the target occurs only after spontaneous opening of the beacon in the lower pathway. The intramolecular quadruplex is represented with a central lateral loop. Similar pathways could have been drawn with a central diagonal loop (as for the intramolecular human telomeric repeat in the presence of Na^+) or with a double reversal loop. Provided that the fluorescent dye (F) and the quencher (Q) are in close proximity in the folded state **1** and enough moved away in the duplex **4**, the photophysical signature associated with the **1**-**4** conversion should be similar.

G-quadruplexes (G4) result from the association of four oligonucleotidic strands held together by the hydrophobic stacking of large, planar, hydrogen-bonded DNA base quartets coordinated to a monovalent cation. A G-quartet, alternatively called a G-tetrad, involves four guanines and a G-quadruplex consists of at least two layers of G-quartets. The presence of the central cation is essential to the structure, but not all cations are equivalent for quadruplex stabilization; their stabilizing power obeys $K^+ > Na^+ \gg Li^+$.[11] The potassium cation, which is very abundant in the intracellular medium, is highly favorable for G-quadruplex formation. Indeed this structure has been reported in cells.[12] Different G-quadruplex structures exist, depending on the orientation of the strands and the *syn*/*anti* conformations of guanines.[13] Although the basic features of G-quartets have been known for more than forty years,[14] it is only in the past decade that the interest in these peculiar structures has increased, due to growing evidences for the implication of G-quadruplex structures in key biological processes.[15−17]

In this manuscript, we evaluate a G-quadruplex-based approach to build molecular beacons (G4-MB). In particular, we examine the opportunities that a G-quadruplex stem could provide to optimize target recognition from both the thermodynamic and the kinetic point of view. Besides a recent report using homo-DNA,[18] i.e., reverse Hoogsteen AA base pairs, G4-MBs are among the first attempts to substitute, in the MB stem, Watson−Crick base pairing by another pairing system. After investigation of the significance of the loop length and of the cation nature on quadruplex stability, we designed a G4-MB with a stem made of 3 quartets and a loop composed of 12 nucleotides. We demonstrate that the latter G4-MB acts as a molecular beacon toward complementary single-stranded DNA targets. In particular, we show, by observing the thermodynamics as well as the kinetics of the recognition process, that discrimination between matched and mismatched sequences can be performed over a larger temperature range than that with classical Watson−Crick MBs. We analyze the origin of this feature, and we eventually discuss the considerations to be taken into account for engineering G4-MBs adapted to more general circumstances.

2. Results

2.1. Design of a G4-MB. In the present account, we introduced the motif for target recognition in the central loop of an intramolecular quadruplex. As shown in the structure displayed in Figure 1, the sequence of an oligonucleotide giving such a G4-MB should contain (i) two lateral portions to form the quadruplex structure as well as a central 10 to 20 base-long loop portion complementary to the target and (ii) a fluorophore−quencher pair located at the termini of the oligonucleotide.

2.1.1. Oligonucleotide Backbone. We used the human telomeric sequence to design the lateral portions that will form a three quartet stem (Figure 1 and Table 1). Such sequences were reported to yield intramolecular quadruplexes with 1 to 7 base-long loops.[13,19] In contrast, no evidence existed for intra-

(11) Williamson, J. R. *Annu. Rev. Biophys. Biomol. Struct.* **1994**, *23*, 703−730.
(12) Schaffitzel, C.; Berger, I.; Postberg, J.; Hanes, J.; Lipps, H. J.; Plückthun, A. *Proc. Natl. Acad. Sci. U.S.A.* **2001**, *98*, 8572−8577.
(13) Hazel, P.; Huppert, J.; Balasubramanian, S.; Neidle, S. *J. Am. Chem. Soc.* **2004**, *126*, 16405−16415.
(14) Gellert, M.; Lipsett, M. N.; Davies, D. R. *Proc. Natl. Acad. Sci. U.S.A.* **1962**, *48*, 2013−2018.
(15) Rangan, A.; Fedoroff, O. Y.; Hurley, L. H. *J. Biol. Chem.* **2001**, *276*, 4640−4646.
(16) Duquette, M. L.; Handa, P.; Vincent, J. A.; Taylor, A. F.; Maizels, N. *Genes Dev.* **2004**, *18*, 1618−1629.
(17) Paeschke, K.; Simonsson, T.; Postberg, J.; Rhodes, D.; Lipps, H. J. *Nat. Struct. Mol. Biol.* **2005**, *12*, 847−854.
(18) Crey-Desbiolles, C.; Ahn, D.; Leumann, C. *Nucleic Acids Res.* **2005**, *33*, e77.
(19) Risitano, A.; Fox, K. R. *Org. Biomol. Chem.* **2003**, *1*, 1852−1855.

Table 1. Names and Sequences (5′-3′ Orientation) of the Oligonucleotides That Were Used in This Study[a]

Name	Sequence
30G	**GGGTTAGGG**TCCTTTGTTTGT**GGGTTAGGG**
30GMB	Fluorescein-**GGGTTAGGG**TCCTTTGTTTGT**GGGTTAGGG**-Dabcyl
13ACA	CACAAACAAAGGA
13AAA	CACAAAAAAAGGA
13ACC	CACAAACAACGGA
F-13ACA	Fluorescein-CACAAACAAAGGA
9C	**CCCTAACCC**
38G	**GGGGGTTAGGGGG**TCCTTTGTTTGT**GGGGGTTAGGGGG**
30con	**GGGTTAGTG**TCCTTTGTTTGT**GCGTTAGTG**
21tel	**GGGTTAGGG**TTA**GGGTTAGGG**
39G	**GGGTTAGGG**TTTTTTCCTTTGTTTGTTTTT**GGGTTAGGG**
36G	**GGGTTAGGG**TTTTCCTTTGTTTGTTTT**GGGTTAGGG**
33G	**GGGTTAGGG**TTTCCTTTGTTTGTT**GGGTTAGGG**
24G	**GGGTTAGGG**TTTGTT**GGGTTAGGG**
21G	**GGGTTAGGG**TGT**GGGTTAGGG**

[a] The G4-MB (30G and the corresponding doubly labeled 5′ fluorescein-3′ dabcyl 30GMB) as well as the complementary oligonucleotides (matched sequence, 13ACA; mismatched sequences, 13AAA and 13ACC) are shown in the tabletop. The bases in bold are involved in the formation of the quadruplex structure, whereas the underlined ones locate the mismatches. The sequences in the middle were used as control oligonucleotides (38G and 30con are 30G analogues that do not unfold and do not contain a quadruplex structure, respectively). The oligonucleotides in the table bottom were studied to probe the effect of the loop length on the beacon stability.

molecular quadruplex formation with a longer loop when we started the present work. We consequently first analyzed the behavior of putative G4 probes with central sequences of different lengths (3 to 21 bases), in the presence of different salts (Table 1).

Figure 2a displays the typical evolution with respect to temperature of the absorbance at 295 nm of a 2 μM solution of 30G, a sequence with a 12 base-long loop, in the presence of 10 mM lithium cacodylate pH 7.2 supplemented with 100 mM LiCl, NaCl, or KCl (see also Figure 1Sa and 1Sb for complementary UV absorption and circular dichroism experiments). One notices the presence of a cation-dependent conformational change associated with the temperature increase. The corresponding thermal differential spectra (TDS) in K^+ and Na^+ buffers are shown in Figure 2b. These TDS spectra were obtained by the difference between the absorption spectra recorded above and below the observed transition. They exhibit the typical pattern of an intramolecular G-quadruplex structure with two positive maxima at 240 and 275 nm and a negative minimum around 295 nm.[20] Thus, the observed transition was suggested to be associated with the melting of an intramolecular quadruplex at a melting temperature denoted as T_m in the following. Formation of a quadruplex was confirmed by the stability dependence of the structure on the nature of the monocation. As expected, the stability of the G4-MB quadruplex was the lowest in LiCl, intermediate in NaCl, and the highest in KCl (T_m = <15, 46, and 55 °C, respectively, Figure 2a and Table 2). Concentration-independent melting temperatures confirmed that the folding process was intramolecular (Supporting Information; Figure 2S). Similar observations were made throughout the series of oligonucleotides devoted to probe the effect of the loop length on the G4-MB stability. Table 2 summarizes the thermodynamic data that were collected from the analysis of the UV melting experiments.[21]

Figure 3 shows the evolution of T_m as a function of the number n of nucleotides in the loop portion for 2 μM oligonucleotide solutions in 100 mM KCl, 10 mM lithium cacodylate pH 7.2. As previously observed for a limited size range,[13] T_m steadily decreases when the loop length is increased (see also Table 1S in the Supporting Information). The corresponding evolutions of the enthalpic $\Delta_{21}H°$ and entropic $T\Delta_{21}S°$ contributions to the Gibbs free energy $\Delta_{21}G°$ associated with the formation of the quadruplex motif at 298 K are displayed in Figure 3S (see also Table 1S in the Supporting Information). We observed enthalpy−entropy compensations that are often observed in families of closely related species submitted to identical reactions;[22] they have also already been studied for nucleic acid associations.[23,24]

Mg^{2+} cations affect DNA duplex stability but have been reported to marginally alter one of DNA intramolecular quadruplexes.[19] We envisioned that such a feature could facilitate the design of G4-MBs: in addition to the lengths of the loop and of the stem, magnesium(II) concentration could become a relevant parameter to finely tune the difference in melting temperatures associated with the beacon folding and with the probe−target duplex formation, respectively. Thus, we examined

(20) Mergny, J. L.; Li, J.; Lacroix, L.; Amrane, S.; Chaires, J. B. *Nucleic Acids Res.* **2005**, *33*, e138.

(21) Despite the presence of several folded states, a two-level model was proven to be relevant for the analysis of the UV melting curve experiments (eq 1). If the thermodynamic parameters of the different foldamers are similar within experimental errors, the extracted constants hold for all of them. Otherwise, a folded state is more stable than the other ones, and the measured parameters will correspond to it. The significance of the extracted values is discussed in Appendix A of the Supporting Information.

(22) Leffler, J. E.; Grunwald, E. *Rates and Equilibria of Organic Reactions as Treated by Statistical, Thermodynamic, and Extrathermodynamic Methods*, reprint; Dover: New York, 1989.

(23) Searle, M. S.; Williams, D. H. *Nucleic Acids Res.* **1993**, *21*, 2051−2056.

(24) Strazewski, P. *J. Am. Chem. Soc.* **2002**, *124*, 3546−3554.

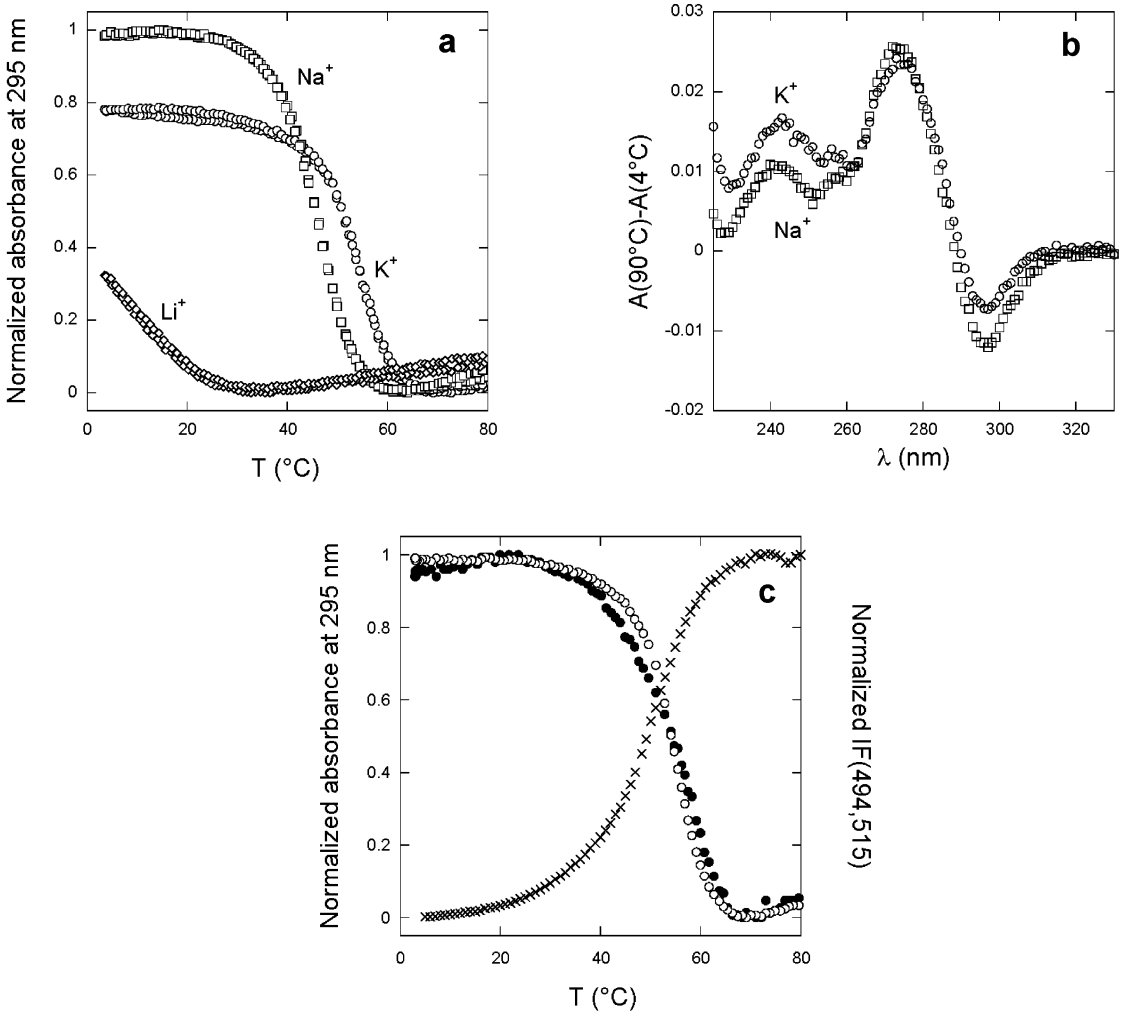

Figure 2. (a) Quadruplex folding/unfolding transitions followed by absorbance and fluorescence spectroscopies. Change in the absorbance at 295 nm (*A*) with respect to temperature of a 2 μM 30G solution in 10 mM lithium cacodylate pH 7.2 in the presence of 100 mM KCl (○), NaCl (□), or LiCl (◇). For comparison, the maximum and minimum values in the presence of NaCl were normalized to 1 and 0, and the values in the presence of LiCl and KCl were correspondingly transformed. (b) Corresponding thermal differential spectra (TDS). (c) Change, with respect to temperature, in the absorbance at 295 nm of 2 μM oligonucleotide solutions (30G, ○; 30 GMB, ●) and in the steady-state fluorescence emission at 515 nm (λ_{exc} = 494 nm) of a 0.2 μM 30GMB solution (×). Buffer: 100 mM KCl, 10 mM lithium cacodylate pH 7.2. Maximum and minimum values were normalized to 1 and 0 for comparison.

the significance of Mg^{2+} on the melting behavior of the investigated G4-MB. Figure 3 shows that the addition of 10 mM $MgCl_2$ to a 100 mM KCl buffer increases the melting temperature of the G4-MB by up to 10 °C. The presence of Mg^{2+} correspondingly alters the thermodynamics of the melting transition (Figure 3S). It is worth noting that, in contrast to the human telomeric sequence 21tel, the quadruplex formed by the closely related 21G sequence is noticeably stabilized in the presence of Mg^{2+} (Tables 1 and 1S). This unexpected observation points out that the loop composition could be important in the stability of the quadruplex and in the interaction with magnesium ions (possibly associated with the preferential formation of different foldamers),[13] at least for small loops.

The preceding results suggest that a G4-MB may accommodate a central loop of up to 21 bases and still be formed at physiological temperature. This observation is significant in relation to the prevalence of putative quadruplex sequences throughout the human genome. Over 370 000 quadruplex-prone sequences were recently found by setting a maximum seven nucleotide length for quadruplex loops;[25,26] our results indicate that this number could be even larger than anticipated.

For the rest of this study, we retained a G4-MB oligonucleotide with a 12 base-long central loop, 30G, and its fluorescently labeled analogue, 30GMB (Table 1).

2.1.2. Fluorophore/Quencher Couple. The choice of the fluorophore/quencher couple relies on both photophysical and functional considerations.[8] Ideally, the transition between the open and the closed G4-MB states should be accompanied by a major change in fluorescence emission. In addition, labeling should not too strongly alter the intrinsic thermodynamic features of the nonlabeled probe. We relied on 30GMB, a labeled analogue of the 30G sequence, bearing fluorescein and dabcyl units at its extremities. The latter fluorophore/quencher pair has been already extensively investigated.[8] Figure 2c displays the evolution with respect to temperature of the absorbance at 295 nm as well as of the steady-state fluorescence emission at 515 nm (λ_{exc} = 494 nm) of 30GMB solutions in 100 mM KCl, 10 mM lithium cacodylate pH 7.2. At the same 2 μM concentration in oligonucleotide, the melting transition observed in UV

(25) Todd, A. K.; Johnston, M.; Neidle, S. *Nucleic Acids Res.* **2005**, *33*, 2901−2907.
(26) Huppert, J. L.; Balasubramanian, S. *Nucleic Acids Res.* **2005**, *33*, 2908−2916.

Table 2. Thermodynamic Data Associated with the Intramolecular Formation of a Three Quartet Quadruplex Motif for the 30G and 30GMB Sequences, as Extracted from UV Melting Experiments Using a Two-State Model (Appendix A in the Supporting Information)[a]

sequence	$T_m \pm 1$ (°C)	$\Delta_{21}H° \pm 20\%$ (kJ mol^{-1})	$\Delta_{21}S° \pm 20\%$ (J mol^{-1} K^{-1})	$\Delta_{21}G°(298\ K) \pm 20\%$ (kJ mol^{-1})
30G (KCl)	55	−250	−770	−22
30G (KCl,$MgCl_2$)	63	−260	−760	−29
30G (NaCl)	46	−220	−700	−15
30G (LiCl)	<15	*b*	*b*	*b*
30GMB (KCl)	53	−180	−550	−16
30GMB (KCl,$MgCl_2$)	64	−210	−640	−25
30GMB (NaCl)	45	−150	−470	−10
30GMB (LiCl)	<10	*b*	*b*	*b*

[a] Experimental conditions: 2 μM oligonucleotide in 10 mM lithium cacodylate buffer (pH 7.2) containing 100 mM KCl, NaCl, or LiCl, in the presence or in the absence of 10 mM $MgCl_2$. [b] Not determined (T_m too low).

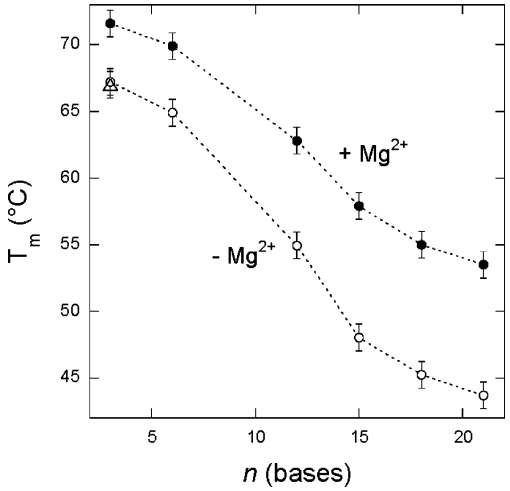

Figure 3. Influence of the loop length on the quadruplex stability. Change in the melting temperature T_m with respect to the number of nucleotides in the loop portion of the G4-MB for 2 μM oligonucleotide solutions in 10 mM lithium cacodylate pH 7.2 supplemented with 100 mM KCl in the presence (●) or in the absence (○) of 10 mM $MgCl_2$. The corresponding data for the 21tel sequence are displayed as a triangle (identical T_m in the absence and in the presence of 10 mM $MgCl_2$; Table 1S).

absorption satisfactorily compares with the one in fluorescence emission: both observables can be equally used to monitor the conformational transition. In agreement with previous reports,[27] we observed that the presence of labels does not forbid the quadruplex formation. In fluorescence emission, the stem melting is accompanied by an increase of fluorescence emission from the fluorescein (16-fold at 515 nm upon excitation at 494 nm). This observation agrees with the expected increase of the average distance between the fluorophore and the quencher when going from the folded state to the random coil (Table 1).

Despite the fair agreement between the melting temperatures of the labeled and nonlabeled sequences (T_m = 53 °C for 30GMB and T_m = 55°C for 30G), Table 2 shows that the enthalpy $\Delta_{21}H°$ and the entropy $\Delta_{21}S°$ of the labeled oligonucleotide are less favorable for quadruplex formation. Such alterations associated with labeling have already been reported.[27] In relation with G4-MB design process, sequence optimization should thus include the terminal labels from the beginning.

2.1.3. Opening/Closing Dynamics. The folding dynamics of a molecular beacon is a significant parameter that determines the time scale of the response to the targeted oligonucleotide. Therefore, we successively measured the opening and the closing rate constants of 30GMB.

We used two different approaches to measure the folding rate constant of 30GMB, k_{21}, in 100 mM KCl, 10mM $MgCl_2$ buffer at 298 K. We first performed T-jump experiments by adding to the buffer thermostated at 298 K aliquots of 30GMB concentrated solutions thermostated at 353 K: the drop in temperature here is expected to promote quadruplex folding. Figure 4a shows that the T-jump causes a drop in the fluorescence emission from fluorescein in less than 1 min. Such an observation is in line with the quadruplex formation that brings the fluorophore and its quencher to closer proximity. In contrast to the expected behavior for an isomerization (Appendix B in the Supporting Information), the time-dependence of fluorescence emission could not be fitted by a monoexponential function. However, it is satisfactorily accounted for by a biexponential function leading to two folding rate constants: $k_{21a} = (2.7 \pm 0.05) \times 10^{-1}$ s^{-1} and $k_{21b} = (4.8 \pm 0.05) \times 10^{-2}$ s^{-1} (relative amplitudes a_{21a} = 45% and a_{21b} = 55%). We also performed isothermal salt-change experiments[28] at 298 K by adding to 100 mM KCl, 10mM $MgCl_2$, 10mM lithium cacodylate buffer pH 7.2 aliquots of 30GMB concentrated solutions in 100 mM LiCl, 10mM $MgCl_2$, 10mM lithium cacodylate buffer pH 7.2 (300-fold dilution): the change in cation, Li^+ to K^+, is responsible for the formation of the quadruplex. As shown in Figure 4a, the fluorescence emission from fluorescein drops in the same time range as that in the T-jump experiment. Again, this time evolution could not be satisfactorily fitted with a monoexponential function. The biexponential fit now leads to $k_{21a} = (2.7 \pm 0.05) \times 10^{-1}$ s^{-1} and $k_{21b} = (3.6 \pm 0.05) \times 10^{-2}$ s^{-1} (relative amplitudes a_{21a} = 60% and a_{21b} = 40%). These values are in reasonable agreement with the values found in T-jump experiments.

To estimate the opening rate constant k_{12} in 100 mM KCl, 10mM $MgCl_2$ buffer at 298 K, we studied 30GMB hybridization with a short DNA oligonucleotide, 9C, that is complementary to the sequence of the stem but not of the loop (Table 1).[28−31] Provided that pairing of 9C with the 30GMB open state occurs faster than opening of the 30GMB closed form,[32] hybridization kinetics of the 9C trap will be limited by the kinetics of quadruplex opening. As shown in Figure 4b, the addition of a 100 molar excess of 9C to a 20 nM 30GMB G4-MB solution in 100 mM KCl, 10mM $MgCl_2$, 10mM lithium cacodylate buffer pH 7.2 at 298 K causes a slow increase in fluorescence emission

(27) Mergny, J. L.; Maurizot, J. C. *ChemBioChem* **2001**, *2*, 124−132.

(28) Raghuraman, M. K.; Cech, T. R. *Nucleic Acids Res.* **1990**, *18*, 4543−4552.
(29) Zhao, Y.; Kan, Z.-Y.; Zeng, Z.-X.; Hao, Y.-H.; Chen, H.; Tan, Z. *J. Am. Chem. Soc.* **2004**, *126*, 13255−13264.
(30) Ying, L.; Green, J. J.; Li, H.; Klenerman, D.; Balasubramanian, S. *Proc. Natl. Acad. Sci. U.S.A.* **2003**, *100*, 14629−14634.
(31) Green, J. J.; Ying, L. M.; Klenerman, D.; Balasubramanian, S. *J. Am. Chem. Soc.* **2003**, *125*, 3763−3767.

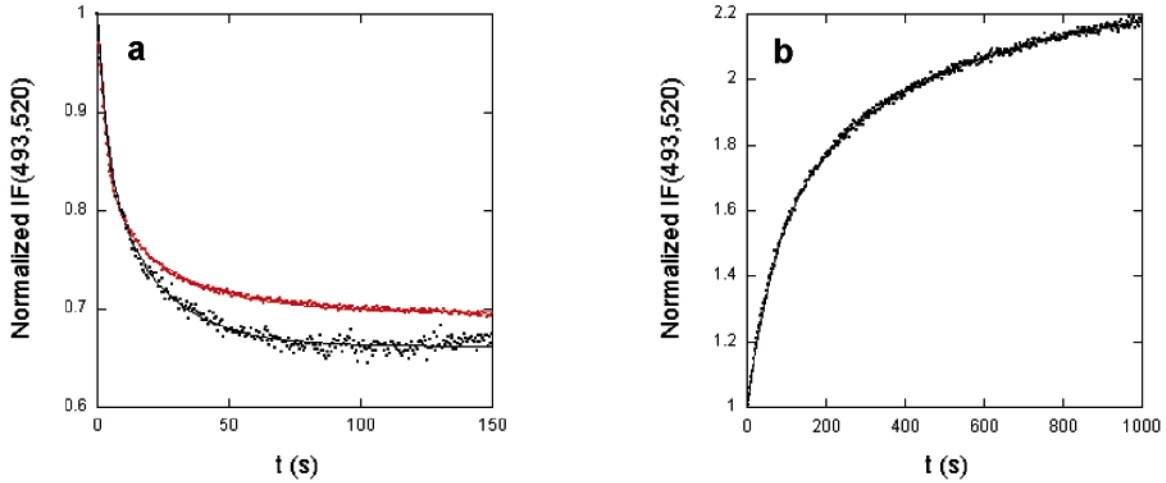

Figure 4. Quadruplex folding/unfolding kinetics. (a) Formation kinetics of the quadruplex stem of 30GMB at 298 K. T-jump experiment (black markers): an aliquot of concentrated solution of unfolded 30GMB at 353 K is 300-fold diluted at $t = 0$ s in 100 mM KCl, 10mM $MgCl_2$, 10mM lithium cacodylate buffer pH 7.2 at 298 K. Salt change experiment (red markers): an aliquot of concentrated solution of unfolded 30GMB in 100 mM LiCl, 10mM $MgCl_2$, 10mM lithium cacodylate buffer pH 7.2 is 300-fold diluted at $t = 0$ s in 100 mM KCl, 10mM $MgCl_2$, 10mM lithium cacodylate buffer pH 7.2 at 298 K. Final concentration in 30GMB is 100 nM. (b) Unfolding kinetics of 30GMB at 298 K in 100 mM KCl, 10 mM $MgCl_2$, 10 mM lithium cacodylate buffer pH 7.2. A 100 molar excess of 9C was added at $t = 0$ s to a 20 nM 30GMB solution in 100 mM KCl, 10 mM $MgCl_2$, 10 mM lithium cacodylate buffer pH 7.2 at 298 K. Markers: experimental points. Lines: biexponential fits. $\lambda_{exc} = 493$ nm; $\lambda_{em} = 520$ nm. The fluorescence signal is normalized at $t = 0$.

from fluorescein. This observation agrees with the quadruplex disruption that moves away the fluorophore from its quencher. Again, the corresponding time evolution of the fluorescence emission could not be fitted by a monoexponential function, but it was satisfactorily accounted for by a biexponential fit giving $k_{12a} = (1.9 \pm 0.04) \times 10^{-3}$ s^{-1} and $k_{12b} = (1.4 \pm 0.05) \times 10^{-2}$ s^{-1} (relative contributions $a_{12a} = 60\%$ and $a_{12b} = 40\%$). The latter rate constants are associated with 1−10 min half-life times that are slightly shorter than that of the intramolecular human telomeric quadruplex under nearly identical conditions.[29,31,33] Such results are in agreement with the observations made for regular MBs: the opening rate depends on the length and on the composition of the stem but is relatively insensitive to loop composition.[34,35]

In principle, the unsuccessful monoexponential fits of the 30GMB folding/unnfolding data could reveal multistep mechanisms or/and the presence of at least two different G4-MB polymorphs. In fact, such a polymorphism has already been observed for the human intramolecular telomeric quadruplex,[36−38] and the kinetic behavior of both subpopulations was even resolved:[30,39] similarly 30GMB could exhibit multiple conformations (parallel, antiparallel or mixed) in solution.[13] In relation to this feature, a distribution of 30GMB photophysical properties as well as of the thermodynamic/kinetic constants would be expected: such a diversity could limit the usefulness of G4-based molecular beacons.

We performed a series of complementary electrophoretic experiments to address the polymorphism issue (Appendix C in the Supporting Information). We did evidence several 30G folded states that could at least partially account for the preceding unsuccessful monoexponential fits. At the same time, we showed that the rate constants associated with the opening and closing processes for the different 30G foldamers were contained within a range covering about 1 order of magnitude, which remained much lower than the penalty associated with a mismatch during the recognition process (vide infra): thus the distribution of thermodynamic and kinetic properties within the foldamer population remains narrow enough to most often satisfactorily assimilate the mixture to one species only at the present experimental precision (see also Appendix A in the Supporting Information). Taking into account that the proper design of the fluorophore−quencher couple should yield a significant fluorophore quenching for all the compact G4-MB folded structures, we conclude that the existence of different G4-MB folded states should not prevent the use of G4-MB for discrimination of oligonucleotide sequences.

2.2. 30G/GMB as Probes for Complementary Oligonucleotides. The 30G/GMB sequence was evaluated as a probe toward complementary oligonucleotides: 13ACA is the matched sequence, and 13AAA and 13ACC are two mismatched ones that differ by the position of the mutated base. We successively analyzed the thermodynamic and the kinetic aspects of the recognition.

2.2.1. Thermodynamic Aspects. Duplex Formation Between Unfolded 30G/GMB and Complementary Sequences. In a first step, we investigated the thermodynamics of association between the loop sequence of the 30G/GMB unfolded state and the complementary sequences.

The pairing process was examined in 100 mM LiCl, 10 mM $MgCl_2$, 10 mM lithium cacodylate buffer pH 7.2 at 298 K.

(32) Under the present experimental conditions, the apparent first-order rate constant for pairing between 9C and the 30GMB open state should be about $(1 \times 10^6) \times (2 \times 10^{-6}) = 2$ s^{-1}. The first number corresponds to an order of magnitude of the bimolecular rate constant for pairing between two complementary oligonucleotides in the presence of 10 mM $MgCl_2$ (for instance, we measured $k_{24} = 1.5 \times 10^6$ M^{-1} s^{-1} during the present study). The second number corresponds to the 9C concentration during the experiment. The 2 s^{-1} latter value is much larger than the measured rate constants which can then be attributed to the 30GMB opening process. Additionally, kinetics curves did not evolve anymore when increasing the 9C molar excess from 100 to 1000, proving that trapping is not the limiting step in this concentration range.

(33) Alberti, P.; Mergny, J. L. *Proc. Natl. Acad. Sci. U.S.A.* **2003**, *100*, 1569−1573.
(34) Bonnet, G.; Krichevsky, O.; Libchaber, A. *Proc. Natl. Acad. Sci. U.S.A.* **1998**, *95*, 8602−8606.
(35) Goddard, N. L.; Bonnet, G.; Krichevsky, O.; Libchaber, A. *Phys. Rev. Let.* **2000**, *85*, 2400−2403.
(36) Wang, Y.; Patel, D. J. *Structure* **1993**, *1*, 263−282.
(37) Parkinson, G. N.; Lee, M. P. H.; Neidle, S. *Nature* **2002**, *417*, 876−880.
(38) Lee, J. Y.; Okumus, B.; Kim, D. S.; Ha, T. *Proc. Natl. Acad. Sci. U.S.A.* **2005**, *102*, 18938−18943.
(39) Phan, A. T.; Patel, D. J. *J. Am. Chem. Soc.* **2003**, *125*, 15021−15271.

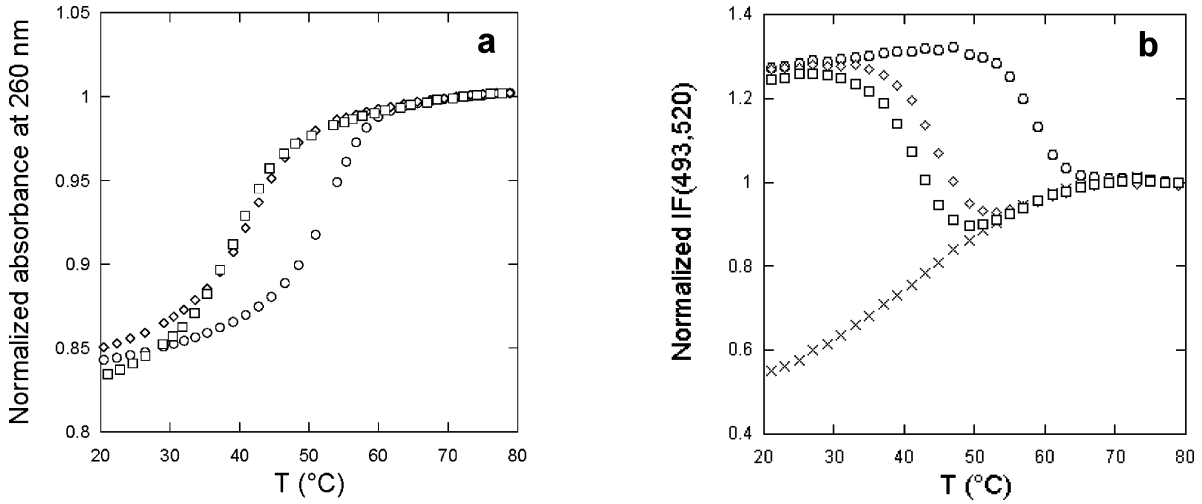

Figure 5. Influence of the mismatches on the duplex stability in Li^+-containing buffer. (a) Temperature dependence of the absorbance at 260 nm of 2 μM 30G in the presence of 1 equiv of 13ACA (○), 13ACC (◇), or 13AAA (□). (b) Temperature dependence of the fluorescence emission from 200 nM 30GMB, alone (×) or in the presence of 6 μM 13ACA (○), 13ACC (◇), or 13AAA (□). $\lambda_{exc} = 493$ nm; $\lambda_{em} = 520$ nm. Only the cooling curves are shown here for clarity; they were normalized at 80 °C by homothetic transformation along the *y*-axis. Solvent: 100 mM LiCl, 10 mM $MgCl_2$, 10 mM lithium cacodylate buffer pH 7.2.

Table 3. Thermodynamic Data Associated with the Formation of a Duplex between the 30G/30con Sequences and the Complementary Sequences 13ACA/13ACC, as Extracted from UV Melting Experiments[a]

sequence	$T_m \pm 1$ (°C)	$\Delta_{24}H° \pm 20\%$ (kJ mol^{-1})	$\Delta_{24}S° \pm 20\%$ (J mol^{-1} K^{-1})	$\Delta_{24}G°(298\ K) \pm 20\%$ (kJ mol^{-1})
30G-13ACA (LiCl)	48	−380	−1070	−61
30G-13ACA (LiCl,$MgCl_2$)	53	−430	−1200	−72
30G-13ACC (LiCl)	37	−300	−850	−47
30G-13ACC (LiCl,$MgCl_2$)	41	−290	−800	−52
30con-13ACA (KCl,$MgCl_2$)	52	−450	−1270	−72
30con-13ACC (KCl,$MgCl_2$)	42	−330	−920	−56

[a] Experimental conditions: 2 μM oligonucleotide in 10 mM lithium cacodylate buffer pH 7.2 containing 100 mM KCl or LiCl, in the presence or in the absence of 10 mM $MgCl_2$.

Under such conditions, the quadruplex does not form. Figure 5a displays the temperature dependence of the absorbance at 260 nm of 2 μM 30G in the presence of 1 equiv of complementary strand. One observes a transition that is interpreted as the melting of an intermolecular duplex. The duplex stability is at the largest with the matched sequence 13ACA; the corresponding duplex exhibits a melting temperature T_m of 53 °C. As expected, the duplexes that involve the complementary mismatched sequences 13ACC and 13AAA are less stable with respective melting temperatures equal to 41 °C and 40 °C. The analyses of the duplex behavior as a function of the concentration in complementary strands yielded the thermodynamic data displayed in Table 3. We additionally investigated in 100 mM KCl, 10 mM $MgCl_2$ buffer at 298 K the association behavior between the complementary sequences and 30con, a control oligonucleotide with the 30G loop but a mutated stem that cannot form the quadruplex. The results from UV melting experiments with 30con in a potassium medium are in fair agreement with the ones obtained with 30G in a lithium medium (Table 3).

Figure 5b displays the temperature dependence of the fluorescence emission in the lithium medium from 200 nM 30GMB, alone or in the presence of 6 μM 13ACA, 13ACC, or 13AAA (at such concentrations, pairing between complementary sequences is complete at 298 K). The fluorescence emission from 30GMB alone increases with temperature. Taking into account that the quantum yield of fluorescein drops when the temperature is increased, the latter behavior probably reflects an endothermic conformational change that moves away the fluorophore and its quencher. In the presence of complementary sequences, one observes a transition that increases fluorescence emission at low temperatures. This result was anticipated from the larger fluorescein−dabcyl distance in the paired duplex rather than in single-stranded 30GMB. The evolution of the melting temperature suggests that the duplex stability decreases in the order 13ACA > 13ACC > 13AAA, which is in agreement with the above UV−vis absorption data.

Recognition Between Folded 30G/GMB and Complementary Sequences. In a second step, we investigated the thermodynamics of association between the loop sequence of the 30G/GMB folded state and the complementary sequences.

Figure 6 displays the evolution with respect to temperature of the fluorescence emission from a 50 nM 30GMB solution in the presence of 6 μM complementary sequences in 100 mM KCl, 10 mM $MgCl_2$ buffer. In view of the slow kinetics of association/dissociation between 30G/GMB and the target sequences (vide infra), the heating and cooling profiles were not perfectly superimposable: only the cooling curves are displayed in Figure 6 for clarity (see also Figure 4Sa for the complete heating/cooling curves).

In the presence of its complementary target 13ACA, the temperature profile of the fluorescence emission exhibits a typical V-shape:[10] the fluorescence emission from fluorescein is large below 40 °C, then it reaches a minimum around 55 °C,

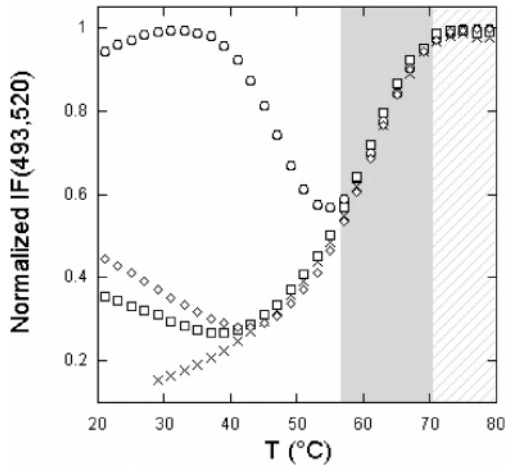

Figure 6. Temperature dependence of the fluorescence emission (normalized by homothetic transformation at 80 °C) from 50 nM 30GMB, alone (×) or in the presence of 6 μM 13ACA (○), 13ACC (◇), or 13AAA (□). λ_{exc} = 493 nm; λ_{em} = 520 nm. Solvent: 100 mM KCl, 10 mM $MgCl_2$, 10 mM lithium cacodylate buffer pH 7.2. Only the cooling curves are shown here for clarity (a slight hysteresis was observed; Figure 4Sa). Target discrimination is possible in the white zone; outside, the duplex is disrupted. In the gray zone, the quadruplex is still partially present, whereas, in the hatched zone, all the nucleotides are single-stranded.

and becomes large again above 70 °C. Such an observation is in line with the following interpretation: (i) above its melting temperature (hatched region), 30GMB is unstructured and dissociated from its target. The distance between fluorescein and dabcyl is large (no fluorescence quenching); (ii) at low enough temperature (here 40 °C or below), 30GMB is opened by pairing with its complementary target. Again, the fluorescein−dabcyl distance is large (no quenching); (iii) at intermediate temperatures, centered around 63 °C (grey region), 30GMB is dissociated from its target and it forms the intramolecular quadruplex structure. The fluorescein−dabcyl distance is reduced, and fluorescence quenching occurs. Note that, above 55 °C, the melting profile of 30 GMB−target mixtures overlap the profile of 30GMB alone.

When the complementary target is replaced by a mismatched sequence, the increase of fluorescence emission at low temperatures is displaced toward lower values. The corresponding shift is more pronounced for 13AAA than for 13ACC. This result is in agreement with the observations that were made with MBs:[40] a point mutation near the center of the probe-binding domain has a larger effect on molecular beacon dissociation than a mutation near the extremities (13AAA versus 13ACC).

The results that were obtained by UV−vis absorption on 30G are in fair agreement with the observations made on 30GMB. Figure 7a displays the temperature dependence of the absorbance at 295 nm of 2 μM 30G in 100 mM KCl, 10 mM $MgCl_2$ buffer. In the presence of 1 equiv of the complementary matched sequence 13ACA, the temperature profile of the absorbance again exhibits a V-shape.[10] The absorbance at 295 nm that signals the presence of the quadruplex motif[20] is at its largest at intermediate temperatures (around 50 °C) and at its lowest below 40 °C and above 70 °C. This behavior is in line with the following sequence, induced by lowering the temperature: (i) unstructured and dissociated complementary oligonucleotides; (ii) quadruplex structuration of 30G; (iii) pairing between complementary strands leading to the duplex formation and disappearance of the quadruplex motif. A similar trend is observed when the complementary target is replaced by a mismatched sequence. Nevertheless, the decrease of the absorbance at 295 nm is displaced toward lower temperatures, and it remains incomplete even at the lowest investigated temperatures.

Experiments were also conducted in the absence of Mg^{2+} to study the influence of divalent cations on the G4-MB function. Figure 7b shows the temperature dependence of the absorbance at 295 nm of 2 μM 30G in 100 mM KCl buffer in the presence of complementary oligonucleotides. With regards to the behavior displayed in Figure 7a, the most noticeable points are (i) the shift of the whole absorbance vs temperature profiles toward lower temperatures and (ii) the destabilization of the duplexes at low temperatures, even in the case of the 13ACA matched sequence for which hybridization remains incomplete.

In relation to using molecular beacons for sequence discrimination of complementary oligonucleotides, the present results show that the G4-MB strategy is attractive. First, the observed behavior is robust. In particular, it does not strongly depend on the presence of the fluorescent terminal labels. This aspect is important because the relevant thermodynamic parameters are significantly affected by labeling. Second, one notices that the temperature range in which the signal arising from G4-MB can be used to differentiate 13ACA from 13ACC and 13AAA is particularly large with regards to that for previously reported MB.[6,10,40] Eventually, we demonstrated that the temperature window for sequence discrimination can be advantageously tuned by altering the concentration of magnesium cation.

2.2.2. Kinetic Aspects. Beyond the above evoked use of G4-MB fluorescence emission at equilibrium for sequence discrimination, we also evaluated the opportunities provided by the time dependence of the G4-MB fluorescence emission with regards to sequence analysis. In fact, the possibility of retrieving sequence information not only from thermodynamics but also from kinetics would be an advantage for selectivity improvements. In this section, we do not extensively report on the kinetic analysis of the recognition between 30GMB and its complementary targets but only emphasize the main results (the details are provided in Appendix B of the Supporting Information).

Two different mechanisms were envisaged to interpret the kinetic experiments (Figure 1). In the first one, denoted **1**-**2**-**4**, the spontaneous opening of 30GMB constitutes a first step which is followed by the bimolecular association of the unfolded sequence with its complementary target. In contrast to previous reports dealing with opening of a rather compact intramolecular quadruplex and subsequent trapping with a complementary oligonucleotide,[19,31,33,41] the presence of a longer loop in 30GMB led us to examine the possible formation of an intermediate **3** in which the target is partially bound to the folded G4-MB. Thus, we also considered a second mechanism, denoted **1**-**3**-**4**, in which the bimolecular reaction of 30GMB with its complementary target gives the adduct **3** that subsequently intramolecularly evolves by beacon opening and duplex formation.[40] The later second step may be or not be assisted by the sequence recognition with regards to the spontaneous opening of 30GMB. We performed several experiments to discriminate between the two preceding mechanisms. The whole collection of exper-

(40) Tsourkas, A.; Behlke, M. A.; Rose, S. D.; Bao, G. *Nucleic Acids Res.* **2003**, *31*, 1319−1330.

(41) Phan, A. T.; Mergny, J. L. *Nucleic Acids Res.* **2002**, *30*, 4618−4625.

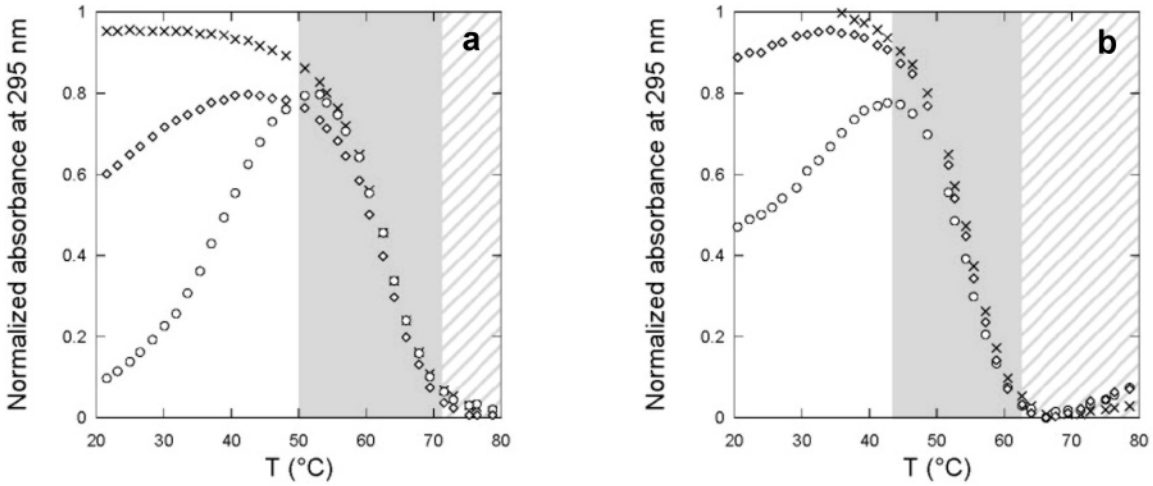

Figure 7. Temperature dependence of the absorbance at 295 nm (normalized between 0 and 1 for the lowest and largest absorbances, respectively) of 2 μM 30G alone (×) or in the presence of 1 equiv of 13ACA (○) or 13ACC (◇). Solvent: 100 mM, KCl 10 mM, lithium cacodylate buffer pH 7.2 in the presence (a) or in the absence (b) of 10 mM $MgCl_2$. Only the cooling curves are shown here for clarity (a slight hysteresis was observed; Figure 4Sb). Target discrimination is possible in the white zone; outside, the duplex is disrupted. In the gray zone, the quadruplex is still present, whereas, in the hatched zone, all the nucleotides are single-stranded.

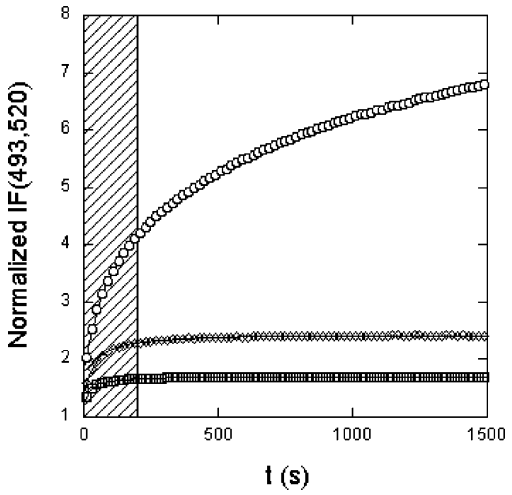

Figure 8. Change in the fluorescence emission from 200 nM 30GMB with respect to time after sudden addition of 1 equiv of 13ACA (○), 13ACC (◇), or 13AAA (□) at 298 K. $\lambda_{exc} = 493$ nm; $\lambda_{em} = 520$ nm. Solvent: 100 mM KCl, 10 mM $MgCl_2$, 10 mM lithium cacodylate buffer pH 7.2. The curves were normalized by dividing the instantaneous fluorescence intensity by the initial fluorescence emission. Sequence discrimination can rely on kinetics beyond the times located in the hatched zone.

imental observations support the **1**-**3**-**4** mechanism to be effective for the matched 13ACA sequence and likely for the mismatched 13ACC and 13AAA ones (see Supporting Information for a detailed discussion). The main conclusions are as follows: (i) over micromolar concentrations in complementary strand, the first step **1**-**3** is fast with regards to the second one **3**-**4**. In relation to the absence of the marked dependence of the rate constants of **3**-**4** on the target sequence, it is **1**-**3** that conveys the sequence selectivity; (ii) under the present experimental conditions, the realization of the second step **3**-**4** is mainly observed beyond a few seconds during the whole **1**-**4** conversion; (iii) the zipping process arising from the duplex formation does not act as a strong driving force for quadruplex disruption.

Figure 8 displays the time evolution of the fluorescence emission from 200 nM 30GMB after addition of 1 equiv of 13ACA, 13ACC, or 13AAA in 100 mM KCl, 10 mM $MgCl_2$ buffer at 298 K. As anticipated from the preceding thermodynamic investigation, the fluorescence emission increases as a function of time. More interestingly, the matched sequence 13ACA is the only complementary one for which we could detect an evolution of the fluorescence signal on a long time scale (beyond 200 s), this kinetic drift being under the control of step **3**-**4**. The preceding observation is significant in relation to using G4-MBs for probing single-strands: sequence analysis here may rely on kinetics. Not only the final value of the fluorescence emission but also its time evolution can discriminate sequences; it exists as a kinetic regime in which a significant evolution of the fluorescence emission is exclusively observed with the matched sequence at the predictable G4-MB opening time scale.

3. Discussion

This study demonstrates that one can obtain efficient molecular beacons that incorporate a G-quadruplex in their stem. Beyond the latter result, the present discussion aims at evaluating the possible advantages and drawbacks associated with choosing a G4 motif instead of a more classical Watson−Crick duplex to build the beacon stem. In relation with thermodynamic aspects, we successively consider the efficiency for sequence discrimination and the design step. Then, we briefly discuss the kinetic aspects.

Sequence discrimination by a beacon usually means obtaining a sequence-specific response after addition of a complementary strand: for instance, one looks for pairing with a perfectly matched oligonucleotide P and no association with a single base mismatched sequence M. In relation with the evaluation of the beacon structure for improved recognition efficiency, two aspects here have to be considered. The first one explicitly deals with recognition selectivity: does a particular beacon design facilitate sequence discrimination at thermodynamic equilibrium by maximizing the ratio K_P/K_M of the association constants between the closed beacon and the oligonucleotides to be probed? When the recognition sequence is located in the beacon loop, one can demonstrate that K_P/K_M only depends on the difference between the Gibbs free energy of association of the unfolded beacon with P and the Gibbs free energy of association of the unfolded beacon with M. In fact, the detailed structure

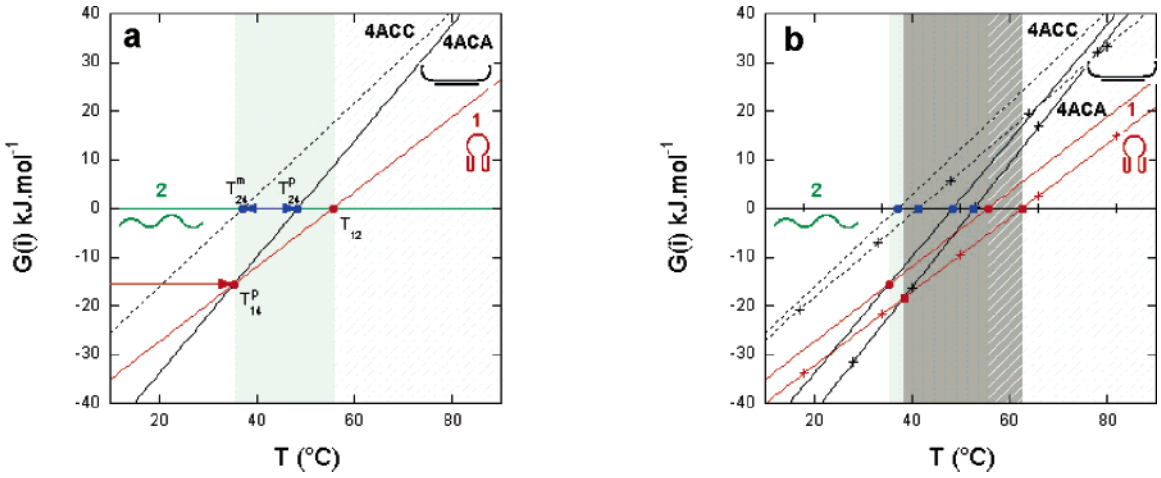

Figure 9. (a) Dependence on temperature of the Gibbs free energy $G(\mathbf{i})$ of the three 30G states: folded (**1**; red solid line), unfolded (**2**; horizontal green solid line), and paired with the complementary target (**4**; black solid line for 13ACA and black dotted line for 13ACC). 30G and its complementary target, 13ACA or 13ACC, are at a $C_0 = 2$ μM total concentration per strand in 100 mM KCl, 10 mM lithium cacodylate buffer pH 7.2. T_{12}, T^p_{14}, T^p_{24}, and T^m_{24} denote the temperatures, respectively, associated with the 30G melting, with the conversion of the folded state **1** to the duplex state **4** for 30G + 13ACA, and with the melting of the central duplexes formed by pairing of 30G with 13ACA and with 13ACC, respectively. In the absence of 30G, sequence discrimination can be envisaged in the $[T^m_{24};T^p_{24}]$ temperature interval (blue arrow). The corresponding range is considerably enlarged when use is made of 30G that adopts its folded state in the gray zone. Sequence discrimination is now possible below T^p_{14}, in the white temperature zone (red arrow). (b) Effect of Mg^{2+}. Dependence on temperature of the Gibbs free energy $G(\mathbf{i})$ of the three 30G states: folded (**1**; red solid line), unfolded (**2**; horizontal green solid line), and paired with the complementary target (**4**; black solid line for 13ACA and black dotted line for 13ACC). 30G and its complementary target, 13ACA or 13ACC, are at a $C_0 = 2$ μM total concentration per strand in 100 mM KCl, 10 mM lithium cacodylate buffer pH 7.2, in the absence (no marker on the lines) and in the presence (crosses on the lines) of 10 mM $MgCl_2$. The temperature range for sequence discrimination is enlarged by adding magnesium cations. See Experimental Section.

of the folded probe does not enter into consideration, and none should bring any distinct advantage. The second aspect deals with the Gibbs free energy associated with the beacon opening that acts as an adjustable penalty which displaces, and increases, the temperature range for mismatch discrimination.[9,10,40] From an experimental point of view, it is desirable to enlarge the latter range. In relation to the present work, the question is whether quadruplex-based beacons bring any new opportunity with regards to traditional MBs.

Figure 9a displays the dependence on temperature of the Gibbs free energy $G(\mathbf{i})$ of the three states **1**, **2**, and **4** for 2 μM 30G and its complementary target, 13ACA or 13ACC, at 2 μM concentration in 100 mM KCl, 10mM lithium cacodylate buffer pH 7.2.[10] At a given temperature, the most stable state is associated with the lowest value of the Gibbs free energy. State **2** is the most stable down to the melting temperature T_{12} of the quadruplex motif. Then, in the case of 30G+13ACA, state **1** is the most stable between T_{12} and T^p_{14} below which the duplex **4** forms. The same succession is anticipated for 30G+13ACC, but the duplex cannot considerably form, even at the lowest temperatures: T^m_{14} lies below the covered temperature range. In relation to using 30G for discriminating the sequence of complementary oligonucleotides, the low slope of the G(**1**) line is responsible for two main advantages of MBs: discrimination can be made at lower temperatures and in a broader temperature range than if it would be directly based on duplex formation **2-4**.

At the considered 2 μM concentration, eqs 7 and 9 (Experimental Section) show that the $G(\mathbf{i})$ positive slopes are essentially governed by the opposites of the negative standard entropies, $\Delta_{21}S°$ and $\Delta_{24}S°$, associated with the formation of the quadruplex and of the duplex, respectively. At the same time, the intercepts between the $G(\mathbf{i})$ lines and the y-axis are governed by the corresponding negative enthalpies of reactions $\Delta_{21}H°$ and $\Delta_{24}H°$. Thus, the efficiency of 30G/GMB results from the relations $\Delta_{24}H° < \Delta_{21}H°$ and $\Delta_{24}S° < \Delta_{21}S°$. In fact, the latter inequalities are anticipated for most structured probes devoted to yield functional MBs. Indeed, $\Delta_{24}H° < \Delta_{21}H°$ is required to enthalpically drive the conversion from state **1** to state **4** which is entropically disfavored. Moreover, the reaction **2-1** is an isomerization, whereas reaction **2-4** reduces by one the number of reactants; one correspondingly expects $\Delta_{24}S° < \Delta_{21}S°$. Taking into account that $\Delta_{24}H°$ and $\Delta_{24}S°$ should be essentially independent of the structure of the folded state of the beacon, the discrimination efficiency of a particular kind of molecular beacon will only depend on the relationship $\Delta_{21}H°(\Delta_{21}S°)$[22] that is characteristic of its stem structure.

Consequently, we compared the present G4-MB with traditional MB exhibiting similar melting temperatures by establishing the corresponding relationship $\Delta_{21}H°(\Delta_{21}S°)$ for different loop lengths. In the absence of extensive experimental investigations, we relied on theoretical predictions based on the Mfold software[42] to get the values of $\Delta_{21}H°$ and $\Delta_{21}S°$ in the case of duplex MB. Figure 9S displays the results. $\Delta_{21}H°$ is linearly dependent on $\Delta_{21}S°$ in the range of investigated stem and loop lengths. In addition, the G4-MBs do not seem to exhibit a behavior that would specifically depart from the one of traditional MBs. Its better efficiency in terms of temperature range for discrimination results from large values of $\Delta_{21}H°$ and $\Delta_{21}S°$; however, the folding simulations indicate that one could probably design as efficient duplex MB by working with longer stems. Here one should notice that the number of bases involved in the stem would then be similar in G4-MB (18) and in MB (16−20). In principle, such large numbers could be a disadvantage because long sequences may participate in nonspecific

(42) Zuker, M. *Nucleic Acids Res.* **2003**, *31*, 3406−3415. The free energies used are from the laboratory of John SantaLucia Jr. (for instance, see: SantaLucia, J. Jr. *Proc. Natl. Acad. Sci. U.S.A.* **1998**, *95*, 1460−1465).

target binding. Nevertheless, G4-MB could be more favorable from the latter point of view. Indeed, the bases involved in the lateral loops may be advantageously replaced by a non-nucleotidic linker, therefore avoiding complementarity to undesired sequences.[43] One may also use inversion probes, as recently proposed for classical beacons.[44]

Although G4-MBs may not significantly be different from MBs as evidenced by the $\Delta_{21}H°(\Delta_{21}S°)$ relationship, they exhibit some advantages for the design step. Indeed, as shown in Figure 9a, an efficient molecular beacon requires setting $T_{12} > T^{p}_{14}$. In the case of traditional MBs, one is left to play with the lengths of the stem and of the loop. In contrast, to reach the appropriate regime with G4-MB, one can additionally play with the concentration of cations, monovalent as well as divalent. This point is illustrated in Figure 9b that displays the evolution of the phase diagram of Figure 9a upon addition of 10 mM $MgCl_2$. In fact, the presence of Mg^{2+} affects $\Delta_{24}H°$ and $\Delta_{24}S°$ much more than it alters $\Delta_{21}H°$ and $\Delta_{21}S°$. As a consequence, one observes here a differential effect leading to an increase of the temperature range for sequence discrimination at a constant sequence of the molecular beacon.

The secondary structure of molecular beacons imposes some kinetic penalty with regard to recognition involving unstructured probes: complex formation proceeds slower, and MB-target association rate constants are generally lower than those reported for hybridization between unstructured probes.[6,40,45] Indeed, an energy barrier must be overcome to open the stem. Opening rate constants that were measured in the present series of G4-MBs are rather small, and the recognition process will be consequently "slow". Such a feature could be a drawback for some applications. At the same time, this study suggests that sequence discrimination could be performed by analyzing the kinetics of beacon opening and not too fast a signal evolution could be here an advantage.

4. Conclusion

G4-MBs provide a versatile strategy for designing efficient molecular beacons. The G4 platform is compatible with building functional MBs that contain long central loops to ensure selective targeting. In the presence of a complementary sequence, the central loop hybridizes and forms a duplex that causes opening of the quadruplex stem, yielding an important change in fluorescence emission. The presence of a single base mismatch hinders this opening process, demonstrating that G4-MB can be efficiently used for oligonucleotide discrimination. With regard to MB containing stems based on a Watson−Crick duplex, G4-MBs offer unprecedented, easy, and predictable new degrees of freedom to tune the experimental conditions for oligonucleotide probing. As an example, the concentration in monovalent as well as divalent cations can be modified to shift the large temperature range in which sequence discrimination can be performed. Eventually, G4-MBs offer an interesting route to building molecular beacons that rely on both thermodynamics and kinetics to perform the discrimination of targeted oligonucleotides.

Beyond the preceding analytical issue, the present study extends the sequence repertoire of quadruplex formation and their implication in biological processes. Furthermore, in the scope of the formation of such structure in vivo, the opening mechanism either by competition or by structure invasion can also be of biological interest, in particular at the telomeres.[46]

5. Experimental Section

Oligonucleotides and Solutions. The sequences of the oligodeoxynucleotides that were used during the present study are given in Table 1. Oligodeoxynucleotides were synthesized by Eurogentec (Seraing, Belgium) or IBA (Göttingen, Germany) on the 0.2 or 1 μmol scale. They were subsequently purified by HPLC, and the doubly labeled 30GMB sequence (fluorescein in 5′ and dabcyl in 3′) was additionally characterized by mass spectrometry. The solution concentrations were estimated by UV absorption using published sequence-dependent absorption coefficients.[47]

The lithium cacodylate buffer was prepared by neutralizing an acid cacodylic solution with lithium hydroxide.

Absorption and Emission Spectra. UV−vis absorption spectra were recorded on 0.2 or 1 cm path length quartz cuvettes on a Kontron Uvikon 940 spectrophotometer thermostated with an external ThermoNeslab RTE111 or ThermoHaake Phoenix C25P1 waterbath.

CD spectra were recorded on a Jasco J810 spectropolarimeter equipped with a Peltier effect-based thermostated cell holder (Jasco France, Nantes, France). A 2 mm optical path quartz cell and an instrument scanning speed of 500 nm/min with a 1 s response time were used for measurements. Each measurement is the average of 6 scans between 220 and 330 nm after an equilibration time of 900 s at each temperature. Spectra were baseline-corrected by subtracting the ellipticity contribution from the buffer and the cell recorded at 20 °C.

The steady-state fluorescence emission spectra were obtained on a Spex Fluoromax3 instrument (Jobin-Yvon Horiba, Chilly-Mazarin, France) thermostated with a ThermoNeslab RTE7 waterbath. Fluorescence emission spectra were collected using a bandwidth of 5 nm and 0.2×1 cm^2 quartz cuvettes containing 600 μL of solution.

Melting Experiments and Thermal Difference Spectra. Absorbance at different wavelengths (245, 260, and/or 295 nm) and fluorescence emission spectra were recorded as a function of temperature that was increased/decreased at a rate of 0.2 °C/min. Melting experiments were typically performed at a concentration of 2 μM per strand. The intramolecular formation of the G-quadruplex beacons was evaluated in the 1−25 μM range.

Thermal difference spectra (TDS) were obtained by the difference between the absorbance spectra from unfolded and folded oligonucleotides that were respectively recorded much above and below its melting temperature (T_m).[20]

Thermodynamic Analysis. Thermal curves were analyzed with a two-state model[21] to extract the standard enthalpy $\Delta_rH°$ and the standard entropy $\Delta_rS°$ of the considered process r under the conditions of Elligham appproximation. In the case of G4-MB, we used

$$\text{G4-MB (open)} = \text{G4-MB (closed)} \tag{1}$$

$$T_m = \frac{\Delta_rH°}{\Delta_rS°} \tag{2}$$

$$K(T) = \frac{1 - \alpha(T)}{\alpha(T)} \tag{3}$$

and in the case of bimolecular associations between complementary oligonucleotides at identical initial concentration per strand C_0, we used

(43) Risitano, A.; Fox, K. R. *Nucleic Acids Res.* **2004**, *32*, 2598−2606.
(44) Browne, K. A. *J. Am. Chem. Soc.* **2005**, *127*, 1989−1994.
(45) Kuhn, H.; Demidov, V. V.; Coull, J. M.; Fiandaca, M. J.; Gildea, B. D.; Frank Kamenetskii, M. D. *J. Am. Chem. Soc.* **2002**, *124*, 1097−1103.
(46) Zaug, A. J.; Podell, E. R.; Cech, T. R. *Proc. Natl. Acad. Sci. U.S.A.* **2005**, *102*, 10864−10869.
(47) Cantor, C. R.; Warshaw, M. M.; Shapiro, H. *Biopolymers* **1970**, *9*, 1059−1077.

$$S + S' = SS' \tag{4}$$

$$T_m = \frac{\Delta_r H^\circ}{\Delta_r S^\circ + R \ln(C_0/2)} \tag{5}$$

$$K(T) = \frac{1 - \alpha(T)}{[\alpha(T)]^2 C_0} \tag{6}$$

In the latter equations, T_m designates the temperature at which the exchanging states are in equal amounts, R is the gas constant, and α measures the proportion of the open (G4-MB) or dissociated (association between complementary oligonucleotides) state.

The experimental data were processed with the Kaleidagraph 3.5 software to extract $\Delta_r H^\circ$ and $\Delta_r S^\circ$ from the Van't Hoff equation: $\ln K(T) = -\Delta_r H^\circ/RT + \Delta_r S^\circ/R$. Then, we wrote $\Delta_r G^\circ = \Delta_r H^\circ - T\Delta_r S^\circ$ to derive the corresponding value of the standard Gibbs free energy.

To extract thermodynamic data, we only analyzed melting profiles that displayed a reversible behavior at the chosen temperature gradient.

Phase Diagrams. The Gibbs free energies of the three states **1**, **2**, and **4** shown in Figure 1 were calculated by assuming the aqueous solutions to be ideal and by taking the same concentration $C_0/2$ for all the different species (the folded quadruplex, the unfolded one, the free complementary target, and the duplex). We additionally considered $G(\mathbf{2}) = 0$ at any temperature.[10] Then, the final expressions of the Gibbs free energies are easily derived:

$$G(\mathbf{1}) = \Delta_{21} H^\circ - T\Delta_{21} S^\circ \tag{7}$$

$$G(\mathbf{2}) = 0 \tag{8}$$

$$G(\mathbf{4}) = \Delta_{24} H^\circ - \left(\Delta_{24} S^\circ + R \ln\frac{C_0}{2}\right) T \tag{9}$$

The phase diagrams that are shown in Figure 9a and 9b were drawn by using corrected values of the 30G thermodynamic data that were collected during the present study. In view of the large incertitudes, we corrected the experimentally derived enthalpies and entropies of reaction, $\Delta_{21}H^\circ(\text{exp})$ and $\Delta_{21}S^\circ(\text{exp})$, that are displayed in Tables 2 and 3 to account for the more precisely measured values of the melting temperatures $T_m(\text{exp})$. In the case of the reaction **2-1**, we adopted $\Delta_{21}H^\circ(\text{corr}) = T_m(\text{exp})\Delta_{21}S^\circ(\text{exp})$ and $\Delta_{21}S^\circ(\text{corr}) = \Delta_{21}S^\circ(\text{exp})$, whereas, for the reaction **2-4**, we wrote $\Delta_{24}H^\circ(\text{corr}) = (1 + x)\Delta_{24}H^\circ(\text{exp})$ and $\Delta_{24}S^\circ(\text{corr}) = (1 + x)\Delta_{24}S^\circ(\text{exp})$ and used eq 5 and $T_m(\text{exp})$ to extract the x value. The corresponding correction was always lower than 7%, which is smaller than the generally accepted experimental incertitudes on enthalpies and entropies.

Kinetic Experiments. The kinetic models and analyses are reported in Appendix B of the Supporting Information. The experimental data were fitted using the KaleidaGraph 3.5 software.

For the slowest kinetics, we relied on fast addition of a reactant in the cuvette under agitation. We correspondingly introduced a time delay t_0 in the fitting laws by replacing t by $(t - t_0)$. The fits typically provided $t_0 \approx 2-3$ s. Such values are in line with the time required for signal stabilization upon dilution of fluorescent samples. For the fastest kinetics, we performed stop-flow experiments on a Spex Fluoromax3 fluorimeter that was equipped with an Applied Photophysics RX2000 rapid kinetics stopped-flow accessory. We used 5-nm-wide excitation and emission slits. The setup requires 120 μL of solution in each reactant for a run. To reduce the noise, data acquisition frequencies were set between 4 and 1 Hz (corresponding to integration times in the 125−500 ms range).

Capillary Electrophoresis. Electrophoretic measurements were performed with a PACE/MDQ (Beckman Coulter Inc, Fullerton, CA) capillary electrophoresis system. This instrument automatically realizes all the steps of the analytical protocols, including capillary conditioning, sample introduction, voltage application, and diode array detection (20 cm from the inlet). Migrations were performed in 50 μm I.D. × 30 cm hydroxypropyl cellulose coated capillaries. New silica capillaries (Polymicro, Phoenix, AZ) were coated using previously described procedures.[48] The running voltage was 10, 12.5, or 15 kV according to these cases. The temperature of the capillary cartridge was set at 20 °C. Samples were introduced hydrodynamically by applying a positive pressure of 0.2 psi for 5 s (c.a. 4 nL) at the inlet end of the capillary. The DNA samples were detected by UV absorbance at 260 nm. Data were processed with the 32 Karat software. Between runs, capillaries were rinsed for 1 min at 20 psi with the running buffer: 220 mM K (or Li) Hepes pH 7.45 (110 mM ionic strength) or 220 mM K (or Li) Hepes pH 7.45 containing 10 mM Mg^{2+} (125 mM ionic strength). All the reagents were obtained from Sigma (Saint Louis, MO) and were of analytical grade.

Acknowledgment. We thank M. Zuker (Rensselaer Polytechnic Institute, Troy, NY), A. De Cian, L. Guittat, J. Gros, B. Saccà, and T. Garestier (MNHN, Paris) for helpful discussions; J. Garel (ENS, Paris) for performing initial kinetic experiments; and C. Tribet (ESPCI, Paris) for giving access to his capillary electrophoresis system. This work was supported by ARC (No. 3365) and EU FP6 (LSHC-CT-2004-502943) MolCancerMed grants (to J.-L.M.); ACI 2003 "Cargos Moléculaires" and ACI-NMAC 2003 "Puces cinétiques" grants from the Ministère de la Recherche et de la Technologie (to L.J., C.G., L.L., A.B., and J.-L.M.); and a Ministère de la Recherche fellowship (to A.E.T.)

Supporting Information Available: Change in the absorbance (Figure 1Sa) and in the ellipticity (Figure 1Sb) with respect to temperature of 30G solutions in 100 mM KCl, 10 mM $MgCl_2$, 10 mM lithium cacodylate buffer pH 7.2. Change in the absorbance at 295 nm with respect to temperature of 30G solutions at different concentrations in 100 mM KCl, 10 mM lithium cacodylate pH 7.2 (Figure 2S). Influence of the loop length on the enthalpic and entropic contributions to the Gibbs free energy associated with the formation of the quadruplex motif (Figure 3S). Temperature dependence of the 30GMB fluorescence emission or of the 30G absorbance in the presence of 13ACA, 13ACC, or 13AAA in 100 mM KCl, 10 mM $MgCl_2$, 10 mM lithium cacodylate buffer pH 7.2 (Figure 4S). Free energy relationships $\Delta_{21}H^\circ(\ \Delta_{21}S^\circ)$ for G4-MB and traditional molecular beacons (Figure 12S). Thermodynamic data associated with the intramolecular formation of a three quartet quadruplex motif for the nonlabeled oligonucleotide sequences (Table 1S). Appendix A: evaluation of the relevance of the thermodynamic parameters extracted from analysis of thermal denaturation curves with a two-level model. Appendix B: detailed analysis of the association kinetics between 30GMB and its complementary targets (including Figures 5S−8S and Tables 2S−4S). Appendix C: electrophoretic measurements (including Figures 9S−11S). This material is available free of charge via the Internet at http://pubs.acs.org.

JA0608040

(48) Shen, Y.; Xiang, F.; Veenstra, T. D.; Fung, E. N.; Smith, R. D. *Anal. Chem.* **1999**, *71*, 5348−5353.